Eng. Sci., 2025, **37**, 1750

Engineered Science
DOI: https://dx.doi.org/10.30919/es1750

The Effects of Impurities on the Physical Properties of Beta-Phase Silicon Nitride: A First-Principles Study

Touwen Fan,[1] Zixiong Ruan,[1] Yue Hong,[1] Bin Deng,[1] Lan Lin,[1] Xianlan Liu,[1] Tiansheng Li,[1,*] Yuanzhi Wu,[1] Heng Luo[2,3,*] and Yuanyuan Zhang[3]

Abstract

Point defects play an important role in the physical properties of materials. In this work, the effects of impurities on the stability, mechanical properties, thermal conductivity and thermodynamics of β-Si_3N_4 have been investigated by first-principles calculations in combination with the Debye model. The results show that, for intrinsic defects, the order of defective formation energy E_f is $V_N < N_{Si} < V_{Si} < Si_N$ in the N-rich side, while in the N-poor side the formation of antisite Si_N becomes facile than the two types before it. The E_f of substitutional defect O_N is always far smaller than that of O_{Si}, while the E_f of group defects O_N-O_{Si} and O_N-V_{Si} are much lower than that of group O_{Si}-V_N in N-rich side. Furthermore, the point defects have a significant effect on mechanical properties, thermal conductivity (TC) κ and Gibbs free energy E_g. Interestingly, the incorporation of substitutional defects Y_{Si}, $(Ce\text{-}Pr)_{Si}$, and $(Tb\text{-}Ho)_{Si}$ would improve the ductility of β-Si_3N_4 based on the acquired G/B results. On the other hand, intrinsic defects V_N, N_{Si}, Si_N and substitutional defects of $(H, C, O)_N$, $(Sc, Y, La, Nd\text{-}Lu)_{Si}$ have the minimal impact on reducing the κ of β-Si_3N_4 and can maintain it up to 200 W/(m·K). These findings are helpful for further investigation of improving the ability of heat transfer and service life for β-Si_3N_4 electronic devices.

Keywords: β-Si_3N_4; First-principles calculations; Point defects; Thermal properties; Mechanical properties.
Received: 26 May 2025; Revised: 25 June 2025; Accepted: 21 September 2025
Article type: Research article.

1. Introduction

Recently, advanced electronic devices have been widely used in various fields, such as automotive electronics, medical devices, and aerospace industries. With the increasing demands of these applications, the growing trends of electronic devises toward the higher power, small volume and high integration as their objectives.[1-3] The higher requirements for these electronic devises will lead to a lot of heat in electronic devises resulting in large thermal stress, which greatly reduces their service life.[4-7] Thus, the outstanding of higher thermal conductivity (TC) and hardness of ceramic substrates become requirements in high-power electronic devices.

The common AlN ceramic substrates exhibit a high TC of 150 W/ (K·m), however, their mechanical properties are insufficient to meet the required bending strength of 350 MPa and fracture toughness of 2.7 MPa·$m^{1/2}$[8] Fortunately, in recent times, there has been a growing interest in silicon nitride Si_3N_4 substrates due to their impressive bending strength of approximately 800 Mpa, remarkable fracture toughness of around ~8 MPa·$m^{1/2}$, lower coefficient of thermal expansion of 3.2×10^{-6} K, high resistivity of $>10^{14}\Omega$·cm, and it has become an indispensable material for supporting advanced semiconductor systems, especially demonstrating irreplaceable advantages in the fields of photonic integration, power module packaging, and high-frequency substrates.[9-15]

To our knowledge, the theoretical average TC of β-Si_3N_4 crystal can reach 320 W/(K·m),[16] however, the β-Si_3N_4 substrates exhibit a lower thermal conductivity of approximately 100 W/(K·m) in practical scenarios due to the presence of point defects, secondary phases, grain boundary films, and porosity, especially in the case of high concentration of oxygen point defects.[11,17] The oxygen atoms can substitute nitrogen sites, resulting in the generation of group defects of O_N+V_{Si}, thereby decreasing the phonon mean free path, and thus decreasing the TC of β-Si_3N_4.[18,19] In addition, point defects have a significant impact on the mechanics and thermodynamics of materials.[20-22] Meanwhile, the sinter

[1]*Research Institute of Automobile Parts Technology, Hunan Institute of Technology, Hengyang, 421002, China*
[2]*College of Materials Science and Engineering, Hunan University, Changsha, 410082, China*
[3]*Xinjiang Xianghe New Materials Technology Co., Ltd, Hami, 839000, China*
[*]*Email*: 2021001018@hnit.edu.cn (T. Li),
luoheng1020@yeah.net (H. Luo)

additives of rare earth (RE), such as Y_2O_3, Yb_2O_3, CeO_2, elements in experiments as the most common approach can significantly improve the TC of β-Si_3N_4 semiconductor ceramics.[23,24]

Mikito *et al*. have investigated the TC of β-Si_3N_4 with a series of rare earth (RE=La, Nd, Gd, Y, Yb and Sc) oxide additive.[25] Their results showed that with the decrease of the ionic radius of RE elements, the TC of Si_3N_4 ceramics will increase owing to an increasing cationic field strength to decrease lattice oxygen content. Yokota *et al*.[26] have sintered high-purity β-Si_3N_4 powder at a temperature of 1900 °C with the sintering agent, consisting of 10% mass fraction Yb_2O_3 and 2% mass fraction ZrO_2. The experiments were meticulously categorized into two groups, with group B subjected to annealing at a temperature of 1900 °C. The results showed that under longer sintering time of ~36 hours and additional annealing treatment, the TC of group B is about 50% higher compared to group A without annealing, reaching 150 W/ (K·m) due to significant grain growth and reduced lattice defects. Dai *et al*.[27] proposed a sintering method: (1) about 0.4 wt.% Al was added to Si powder; (2) then, the mixed powder underwent nitration reaction at 1400 °C; (3) finally, the obtained β-Si_3N_4 sample was sintered at 1900 °C. The results demonstrated a decrease in fracture toughness from 7.3 to 6.0 MPa·$m^{1/2}$ with an increase in Al content, accompanied by a decline in TC from 91.9 to 58.0 W/ (K·m), which can be attributed to the dissolution of Al in β-Si_3N_4.

Although we have learned that the TC and mechanical property of β-Si_3N_4 are influenced by intrinsic defects and exotic impurity atoms, a comprehensive understanding of the atomic-level intrinsic factors is still lacking. Furthermore, the impacts of point defects on the thermodynamic properties, such as Gibbs free energy, thermal expansion coefficient, etc. have not been proposed. And the potential relation between TC, mechanical property and thermodynamic properties of β-Si_3N_4 and the positions of impurity elements in the periodic table hasn't been suggested. To date, it's still difficult to investigate the effects of point defects on the TC β-Si_3N_4 in experiment due to the complex operation and multivariate environment. In recent years, with the development of modern computer technology, the theoretical identification, *e.g.*, first-principles calculations, in complicate materials has been becoming a useful method for the investigation and applied in materials such as metals, semiconductors, high entropy alloys and 2D materials.[28-36]

Lu *et al*.[37] have used the first-principles calculation to investigate the effects of vacancies on structural stability of β-Si_3N_4. Their results show that the N vacancy V_N is easier to form than the Si vacancy V_{Si} as the vacancy formation energy of V_{Si}, 12.56 eV, is larger than that of V_N, 3.38 eV, under the same thermodynamic conditions. Yang *et al*.[38] have studied the effect of La element on the oxygen dissolving in β-Si_3N_4 by fixing La at the surface of β-Si_3N_4 based on first-principles calculations. They pointed out that oxygen atom favors staying in the central vacancies of β-Si_3N_4, and the doping of La atom can effectively immobilize oxygen on the surface of β-Si_3N_4, thereby preventing the diffusion of oxygen impurities into the inner lattice. The findings further demonstrated that the presence of 1.429 at. % oxygen resulted in a reduction of 35.28% and 18.78% in the TC and shear modulus, respectively, of β-Si_3N_4. Very recently, Li *et al*[39] adopted first-principles combing with phonon's Boltzmann transport equation within the relaxation-time approximation (RTA) to calculate TC of β-Si_3N_4. Their results showed that the TC of pure β-Si_3N_4 can reach 325.06 W/ (m·K).

Based on the above analysis, despite the frequent occurrence of nonmetals (NMs) and rare earth elements (REs) in β-Si_3N_4, there is currently no comprehensive and clear explanation of the competitive relationship between these atoms for replacing vacancies in Si_3N_4. This is essential to avoid excessively reducing thermal conductivity at the atomic level. In our work, we firstly calculated the defective formation energy of intrinsic (V_{Si}, V_N, Si_N, N_{Si}) and impurities defects, including nonmetal (NM) and rare earth (RE) elements substitutional (NM_N, RE_{Si}) defects based on first-principles calculation, and then the mechanical parameters of defects containing β-Si_3N_4 ceramic was discussed by the energy-strain method. Further, the effects of defects on TC of β-Si_3N_4 was obtained by using a simple formula from the spectral specific heat integrated. Finally, the effects of defects on the thermodynamics have been discussed using the Debye temperature. All calculated defective formation energy, mechanical parameters, TC and Gibbs free energy were associated with the positions of impurity elements in periodic table.

2. Computation detail

In this work, we employed the density functional theory (DFT) in the Kohn–Sham theoretical framework as implemented in the Vienna ab initio Simulation Package (VASP) with the 5.4.4 version.[40] Meanwhile, The projector augmented wave (PAW)[41] method and Perdew–Burke–Ernzerh of (PBE) version of generalized gradient approximation (GGA)[42] was employed to calculate the total energy of models in VASP codes. In the processing of calculation, the cutoff energy of plane wave basis of 350 eV, and the PAW_GGA pseudopotentials of NM (NM=H, B, C, N, O, F, Si), RE (RE=Sc, RE_sv=Y_sv, RE_3=La-Lu) were adopted, respectively. The system of 2×2×2 supercell containing 112 atoms was used to construct a series of modes of substitution of impurities and intrinsic defects for bulk materials, and Brillouin zone sampling was performed using the Gamma centered Monkhorst–Pack method[43] with 3×3×6 k-point mesh. The electronic self–consistence convergency criterion for electron iteration was 10^{-6} eV/atom; the ground-state geometries were relaxed via conjugate gradient (CG) minimization until the Hellman-Feymann forces[44] on each atom were less than 0.01 eV/Å.

3. Results and discussion

3.1 The stability of defects

To evaluate the relative stability of defects in β-Si_3N_4, we have constructed the defective model, as shown in Fig. 1(a) visualized by the software VESTA.[45] In β-Si_3N_4, the typical intrinsic defects usually consist of four types: vacancies V_{Si}, V_N and antisite defects Si_N, N_{Si}. The substitutional impurity defects can be classified into two categories, namely the non-metallic elements substitution (NM_N) and rare earth elements replacement (RE_{Si}). In Fig. 1(a), the red and orange balls represent the substitution or removal of N and Si sites, respectively. Further, the defective formation energy, a commonly used stability parameter, is determined by calculating the energy difference between a defective and a perfect supercell:

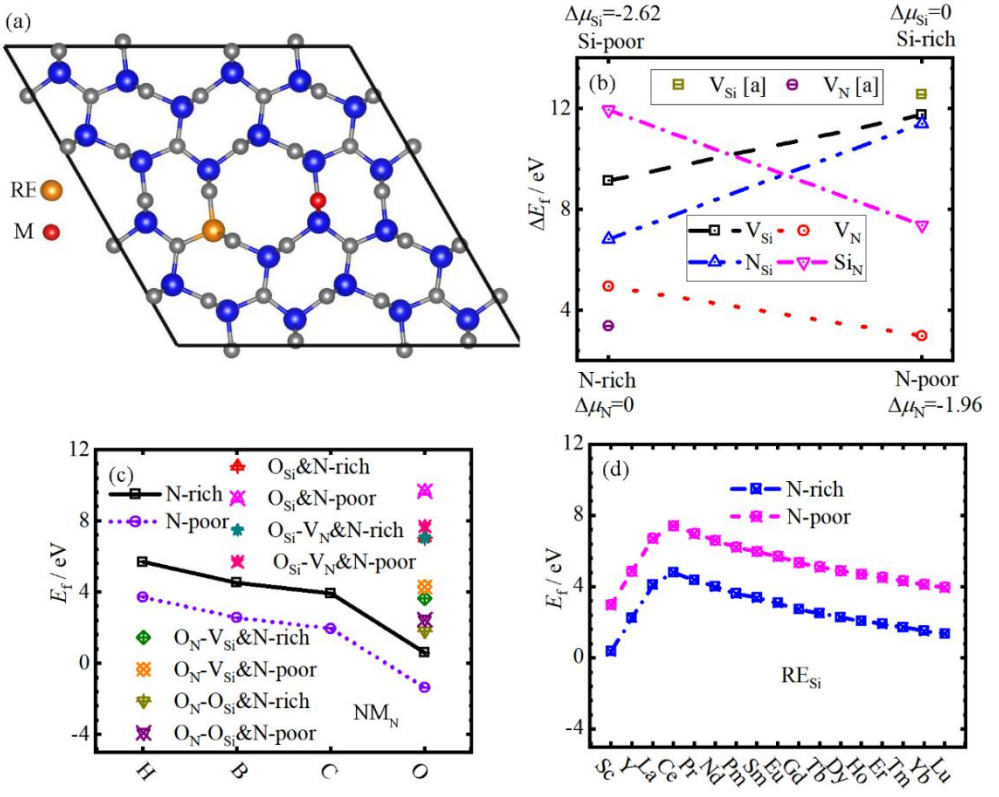

Fig. 1: (a) The defective model; (b) The E_f of intrinsic defects as a function of chemical potential; The E_f of (c) NM_N and (d) RE_{Si} as a function of atomic number, respectively.
Note: the ref. [a] is from the calculated results of Lu *et al*.[37]

$$E_f = E_d - E_p - \sum_i n_i \mu_i \quad (1)$$

In Eq. (1), where E_p and E_d are the total energies of the perfect and defective supercells, respectively. n_i and μ_i are the number of atoms added (n_i>0) or removed (n_i<0) and corresponding chemical potential of specific species, respectively. The chemical potential of specific species plays an important role in β-Si_3N_4. To stabilize β-Si_3N_4 instead of forming bulk Si and gas N_2, the chemical potential μ_i needs to satisfy the following Eq. (2)-(4):

$$3\Delta\mu_{Si} + 4\Delta\mu_N = \Delta H_f(Si_3N_4) \quad (2)$$

$$\Delta\mu_{Si} = \mu_{Si} - \mu_{Si}^0 \leq 0 \quad (3)$$

$$\Delta\mu_N = \mu_N - \mu_N^0 \leq 0 \quad (4)$$

where μ_{Si}^0 and μ_N^0 are the energy of single atom for the Si bulk and N_2 gas, respectively.

Under the N-rich condition corresponding to Si-poor, the N chemical potential μ_N is equal to μ_N^0, following as Eq. (5):

$$\mu_N = \mu_N^0 \quad (5)$$

Thus, the Si chemical potential μ_{Si} can be calculated by inserting $\Delta\mu_N = 0$ into the Eq. (2), and it can be obtained as following Eq. (6):

$$\mu_{Si} = \frac{1}{3}\Delta H_f(Si_3N_4) + \mu_{Si}^0 \quad (6)$$

And the opposite condition (N-poor corresponding to Si-rich), the $\Delta\mu_{Si}$ also is equal to 0 ($\mu_{Si} = \mu_{Si}^0$. Therefore, μ_N can be calculated by Eq. (7):

$$\mu_N = \frac{1}{3}\Delta H_f(Si_3N_4) + \mu_N^0 \quad (7)$$

To investigate the effects of point defects on the TC of β-Si_3N_4, the lattice constant a_0 and the formation energy E_f of vacancies V_{Si}, V_N, antisite defects Si_N, N_{Si}, substitutional impurity elements NM_N and RE_{Si} are firstly calculated, and results are summarized in Table 1. It can be seen that, the

calculated lattice constant a_0 is in good agreement with the experimental and theoretical predicted results with the maximum errors no more than 2%,[37,46,47] demonstrating the accuracy and dependability of the work. However, the maximum error of formation energy E_f between this work and previous results exceeds 1 eV;[37] the discrepancy may arise from the disparity in reference energy for a single N atom compared to previous studies. The energy of -8.269 eV for a single nitrogen atom and -5.418 eV a single silicon atom originates from gas N_2 and bulk Si, respectively.

Clearly, from Table 1, one can see that the E_f of O_N is always much lower than that of O_{Si}, regardless of the N-rich and N-poor conditions (corresponding to Si-poor and Si-rich, respectively), meaning that it's difficult for O atoms to occupy the position of Si in β-Si_3N_4. For double defects, the E_f of combinations O_N-O_{Si} and O_N-V_{Si} are much lower than that of group O_{Si}-V_N. To explicitly articulate the correlation among intrinsic defects, V_N, V_{Si}, N_{Si}, Si_N, and special environment factors, we have calculated the formation energy difference of intrinsic defects under both N-rich ($\Delta\mu_N$=0, $\Delta\mu_{Si}$=-2.62) and N-poor ($\Delta\mu_N$=-1.96, $\Delta\mu_{Si}$=0) conditions, and the main results

Table 1: The calculated lattice constants 2*a* (Å), 2*b* (Å), 2*c* (Å), defective formation energy E_f (eV) and local lattice distortion δ (%) in β-Si_3N_4.

Defects	2*a*	2*b*	2*c*	E_f		δ
				N-rich	N-poor	
SiN	15.100 15.152[46] 15.290[37]	15.100 15.152[46] 15.290[37]	5.778 5.748[46] 5.840[37]	-	-	-
V_N	15.107	15.061	5.784	4.95 3.38[37]	2.99	4.64×10^{-4}
V_{Si}	15.117	15.113	5.772	9.14	11.76 12.56[37]	1.13×10^{-3}
N_{Si}	15.088	15.078	5.782	6.82	11.39	7.95×10^{-4}
Si_N	15.108	15.152	5.804	11.95	7.37	5.30×10^{-4}
H_N	15.145	15.103	5.760	5.70	3.73	2.98×10^{-3}
B_N	15.113	15.142	5.793	4.53	2.56	8.61×10^{-4}
C_N	15.102	15.121	5.786	3.93	1.97	1.32×10^{-4}
O_N	15.114	15.105	5.782	0.60	-1.36	9.27×10^{-4}
O_{Si}	15.096	15.134	5.783	7.05	9.67	2.65×10^{-4}
O_N-O_{Si}	15.122	15.104	5.780	1.82	2.47	1.46×10^{-3}
O_N-V_{Si}	15.096	15.086	5.775	3.65	4.31	2.65×10^{-4}
O_{Si}-V_N	15.082	15.066	5.777	7.05	7.71	1.19×10^{-3}
Sc_{Si}	15.196	15.113	5.793	0.37	2.99	6.36×10^{-3}
Y_{Si}	15.221	15.122	5.796	2.25	4.87	8.01×10^{-3}
La_{Si}	15.248	15.128	5.795	4.11	6.73	9.80×10^{-3}
Ce_{Si}	15.248	15.136	5.798	4.81	7.43	9.80×10^{-3}
Pr_{Si}	15.243	15.136	5.797	4.38	6.99	9.47×10^{-3}
Nd_{Si}	15.237	15.137	5.797	4.00	6.62	9.07×10^{-3}
Pm_{Si}	15.232	15.136	5.796	3.62	6.24	8.74×10^{-3}
Sm_{Si}	15.229	15.135	5.796	3.38	5.99	8.54×10^{-3}
Eu_{Si}	15.227 15.502[47]	15.132 15.393[47]	5.796	3.09	5.71	8.41×10^{-3}
Gd_{Si}	15.224	15.130	5.796	2.75	5.37	8.21×10^{-3}
Tb_{Si}	15.222	15.127	5.796	2.51	5.13	8.08×10^{-3}
Dy_{Si}	15.221	15.125	5.796	2.29	4.91	8.01×10^{-3}
Ho_{Si}	15.219	15.122	5.796	2.09	4.71	7.88×10^{-3}
Er_{Si}	15.219	15.120	5.796	1.91	4.53	7.88×10^{-3}
Tm_{Si}	15.218	15.118	5.796	1.73	4.34	7.81×10^{-3}
Yb_{Si}	15.216	15.117	5.796	1.52	4.14	7.68×10^{-3}
Lu_{Si}	15.216	15.115	5.796	1.36	3.98	7.68×10^{-3}

are depicted in Fig. 1(b). It is found that in N-rich region, the order of E_f is $V_N < N_{Si} < V_{Si} < Si_N$; whereas in the N-poor region, the order of E_f is $V_N < Si_N < N_{Si} < V_{Si}$, indicating that the formation of V_N is consistently facilitated under both N-rich and N-poor conditions. From the results of order of E_f, in N-rich side, Si_N and V_{Si} are more difficult to form than N_{Si}, whereas Si_N is easier to form in N-poor side. In addition, the local lattice distortion δ between the solute atoms and Si_3N_4 matrix produces a hardening effect, and can be defined as: $\delta = \frac{a_{def}-a_{per}}{a_{per}} \times 100\%$, where a_{def} and a_{per} are the lattice constants of the defect compounds and pure Si_3N_4, respectively, as also listed in Table 1. From the results, it can be seen that a larger atomic radius would cause larger distortion, leading to better solid solution strengthening effect.

Furthermore, we have illustrated the calculated E_f of substitutional defects NM_N and RE_{Si} in β-Si_3N_4 as a function of atomic number in Fig. 1(c-d) for both N-rich and N-poor conditions. One can see that for both NM_N and RE_{Si} in β-Si_3N_4, the variation trends of E_f exhibit consistent patterns as the atomic number increases, irrespective of N_2 condition. The evidence clearly demonstrates, the E_f of NM_N decreases linearly from ~5.70 eV for H_N to ~3.93 eV for C_N, and then decreases sharply to ~0.60 eV for O_N. Whereas the E_f of RE_{Si} exhibits a linear increase at first, ranging from ~2.99 eV for Sc_{Si} to ~7.43 eV for Ce_{Si}, and then decreases linearly to ~3.98 eV for Lu_{Si}. The results further show that the E_f of NM_N in N-poor shows a lower value than NM_N in N-rich, while E_f of RE_{Si} in N-rich presents a lower value compared to that of RE_{Si} in N-poor. The findings indicate a higher likelihood of NM atoms replacing N sites in N-poor conditions, while RE atoms are more prone to replace Si sites in N-rich environments.

3.2 The effects on mechanical property

The presence of various point defects in semiconductor ceramics is a common phenomenon, and these defects play a pivotal role in fundamental mechanical parameters, such as the bulk modulus B, shear modulus G, Young's modulus E. These parameters can be calculated from elastic constants Cij,[48], which are derived from the correlation between systemic energy and minor deformation, as following[49,50] Eq. (8):

$$\Delta E = \frac{V_0}{2} \sum_{i,j=1}^{6} C_{ij} \varepsilon_i \varepsilon_j \tag{8}$$

where ΔE is the energy difference between the total energies of nonequilibrium E_s and equilibrium E_0 ; the ε_i and ε_j represent the minor strains associated with indexes i and j, respectively. Generally speaking, the mechanical stability of defective structures is evaluated based on the Born criterion,[51] which distinguishes it from an energy perspective. For hexagonal β-Si_3N_4, the criteria for assessing mechanical stability are calculated as[52, 53] Eq. (9)-(10):

$$C_{44} > 0;\ C_{11} - C_{12} > 0 \tag{9}$$

$$C_{11} \times C_{33} > (C_{13})^2;\ C_{33} \times (C_{11} + C_{12}) > 2(C_{13})^2 \tag{10}$$

Specifically, the G and B are used to determine the ability of materials to resist volume and shape deformation, respectively, and the results of them can be used to derive the values of Vicker's hardness of materials by the empirical formula: $H_v = 2(k^2G)^{0.585} - 3$,[54,55] where $k = G/B$ is Pugh's modulus ratio. Besides, Tian *et al.* also provided another method for calculating hardness for superhard crystals: $H_t = 0.92k^{1.137}G^{0.708}$. The B and G can be calculated based on Voigt-Reuss-Hill's theory[53,54,56] by the following Eq. (11)-(16):

$$B_R = \frac{[(C_{11} + C_{12})C_{33} - 2C_{13}^2]}{(C_{11} + C_{12} - 4C_{13} + 2C_{33})} \tag{11}$$

$$B_V = \frac{[2(C_{11} + C_{12}) + 4C_{13} + C_{33}]}{9} \tag{12}$$

$$G_R = \frac{5[(C_{11} + C_{12})C_{33} - 2C_{13}^2]C_{44}C_{66}}{6B_VC_{44}C_{66} + 2[(C_{11} + C_{12})C_{33} - 2C_{13}^2](C_{44} + C_{66})} \tag{13}$$

$$G_V = \frac{C_{11} + C_{12} - 4C_{13} + 2C_{33} + 12C_{44} + 12C_{66}}{30} \tag{14}$$

$$B = \frac{B_R + B_V}{2} \tag{15}$$

$$G = \frac{G_R + G_V}{2} \tag{16}$$

where G_V, B_V and G_R, B_R are the maximum and minimum values of the polycrystalline elastic moduli from Voigt and Reuss theories, respectively. In Eq. (17), the Young's modulus E and Poisson's ratio ν denote the tensile strength and heterogeneity of materials, and they can be calculated from the G and B:[57-59]

$$E = \frac{9GB}{3B + G};\ \nu = \frac{3B - 2G}{2 \times (3B + G)} \tag{17}$$

In addition, the melting temperature (T_m) of non-cubic systems can be theoretically approximated based on C_{11} and C_{33}, as following Eq. (18):

$$T_m = 354 + 1.5(2C_{11} + C_{33}) \pm 300 \tag{18}$$

The calculated elastic constants C_{ij}, bulk modulus B, shear modulus G, Young's modulus E, Pugh's modulus ratio G/B, Vicker's hardness H_V, Tian's hardness H_t and Poisson's ratio ν are compiled in Table 2 and 3. The achievement of satisfactory consistency is derived from the comparison between experimental and computational results, with an acceptable error margin of 20%. From Table 2, it is found that all defective β-Si_3N_4 compounds meet the above judgment conditions. And all defects would reduce the mechanical modulus B, G, E to a certain extent. Moreover, the modulus G and E of β-Si_3N_4 decorated by group defects O_N-V_{Si} are 102.46 and 257.98 GPa, which are significantly reduced compared to

perfect β-Si_3N_4 of 120.88 and 316.19 GPa, respectively, meaning that the group defects O_N-V_{Si} have a significant effect on the mechanical properties of β-Si_3N_4.[60] The orders of B, G and E for β-Si_3N_4 containing various intrinsic defects are $V_N > N_{Si} > V_{Si} > Si_N$, $V_N > Si_N > N_{Si} > V_{Si}$ and $V_N > Si_N > N_{Si} > V_{Si}$, respectively.

To clearly compare the effects of various types of substituted elements on mechanical properties, the main mechanical parameters of NM_N and RE_{Si} doped β-Si_3N_4 as a function of atomic number is further illustrated in Fig. 2. In Fig. 2(a-b), we can see that the calculated values of G and E of β-Si_3N_4 containing NM_N firstly exhibit a linear increase from 113.92 and 291.71 GPa for H_N to 127.56 and 320 GPa for C_N, followed by a decrease to 115.73 and 298.03 GPa for

Table 2: The calculated elastic constants C_{ij} (GPa) of β-Si_3N_4 containing impurities.

Defects	C_{11}	C_{12}	C_{13}	C_{33}	C_{44}	C_{66}
SiN	432.57	211.53	149.58	588.78	100.62	110.52
	433[62]	195[62]	127[62]	574[62]	108[62]	119[62]
	456±31[63]	158±40[63]	238±21[63]	311±40[63]	144±11[63]	149±40[63]
	411[64]	189[64]	117[64]	568[64]	105[64]	112[64]
V_N	390.74	172.82	90.36	571.67	88.71	108.96
V_{Si}	335.92	159.34	100.68	551.05	68.85	88.29
N_{Si}	367.04	152.90	113.26	561.42	90.74	107.07
Si_N	355.75	152.45	90.99	558.28	98.44	101.65
H_N	383.87	190.36	68.62	571.33	88.79	96.75
B_N	383.62	171.28	55.15	575.47	97.38	106.17
C_N	411.61	194.84	39.09	584.41	99.19	108.38
O_N	393.55	186.76	97.25	559.76	92.15	103.39
O_{Si}	359.48	170.29	42.17	559.72	90.25	94.60
O_N-O_{Si}	369.90	164.12	37.85	565.50	97.20	102.89
O_N-V_{Si}	328.22	181.56	7.54	557.31	81.38	73.33
O_{Si}-V_N	354.24	149.74	10.39	565.22	90.75	102.25
Sc_{Si}	384.58	189.84	85.01	555.89	96.47	97.37
Y_{Si}	335.22	187.37	117.94	549.84	95.16	73.92
La_{Si}	370.62	167.08	85.01	551.76	93.82	101.77
Ce_{Si}	314.49	212.16	90.51	545.63	93.73	51.17
Pr_{Si}	320.20	206.36	91.67	546.16	93.83	56.92
Nd_{Si}	353.88	182.97	98.53	546.70	93.99	85.46
Pm_{Si}	362.40	163.89	107.65	547.30	94.17	99.25
Sm_{Si}	357.34	158.78	120.40	547.66	94.35	99.28
Eu_{Si}	357.92	159.34	124.01	547.61	94.41	99.29
Gd_{Si}	358.75	159.50	126.22	548.66	94.72	99.62
Tb_{Si}	334.74	186.91	125.46	549.43	94.91	73.92
Dy_{Si}	335.95	188.04	122.38	550.02	95.11	73.95
Ho_{Si}	340.30	188.30	123.13	550.64	95.36	76.00
Er_{Si}	344.19	187.85	118.64	551.21	95.58	78.17
Tm_{Si}	353.72	192.06	110.61	551.47	95.75	80.83
Yb_{Si}	352.35	182.73	108.46	552.00	95.86	84.81
Lu_{Si}	371.78	187.55	99.42	552.09	95.94	92.11

Table 3: The calculated the bulk modulus B (GPa), shear modulus G (GPa), Young's modulus E (GPa), Vicker's hardness H_V (GPa), Tian's hardness H_t (GPa), melting temperature T_m, Pugh's modulus ratio G/B and Poisson's ratio ν

Defects	B	G	E	H_V	H_t	T_m±300	G/B	ν
SiN	274.23	120.88	316.19	9.68	10.81	2534.86	0.441	0.308
V_N	228.11	117.03	299.82	11.85	12.55	2383.72	0.513	0.281
V_{Si}	213.75	95.33	248.97	8.18	9.25	2188.33	0.446	0.306
N_{Si}	226.02	113.90	292.56	11.32	12.06	2297.25	0.504	0.284
Si_N	213.65	116.80	296.39	12.98	13.47	2258.65	0.547	0.269
H_N	221.25	113.92	291.71	11.68	12.36	2362.59	0.515	0.280
B_N	211.34	123.03	309.10	14.73	15.01	2368.07	0.582	0.256
C_N	217.06	127.56	320.00	15.31	15.57	2465.43	0.588	0.254
O_N	233.88	115.73	298.03	11.15	11.95	2374.29	0.495	0.288
O_{Si}	198.27	114.42	287.88	13.82	14.12	2272.02	0.577	0.258
O_N-O_{Si}	197.97	122.07	303.78	15.88	15.93	2311.95	0.617	0.244
O_N-V_{Si}	178.35	102.46	257.98	12.69	12.99	2174.63	0.574	0.259
O_{Si}-V_N	179.06	120.24	294.74	17.68	17.37	2264.56	0.672	0.226
Sc_{Si}	226.83	115.86	297.00	11.69	12.40	2341.56	0.511	0.282
Y_{Si}	227.61	99.83	261.28	8.27	9.38	2184.40	0.439	0.309
La_{Si}	217.74	115.61	294.68	12.35	12.94	2293.50	0.531	0.274
Ce_{Si}	216.82	88.22	233.06	6.60	7.89	2115.90	0.407	0.321
Pr_{Si}	217.34	91.81	241.43	7.27	8.47	2133.84	0.422	0.315
Nd_{Si}	222.78	106.91	276.51	10.03	10.91	2235.68	0.480	0.293
Pm_{Si}	224.06	112.28	288.64	11.11	11.86	2262.13	0.501	0.285
Sm_{Si}	226.78	111.02	286.34	10.63	11.46	2247.49	0.490	0.290
Eu_{Si}	228.54	110.75	286.04	10.45	11.31	2249.19	0.485	0.291
Gd_{Si}	229.77	110.91	286.60	10.40	11.27	2253.23	0.483	0.292
Tb_{Si}	230.40	99.05	259.90	7.96	9.12	2182.37	0.430	0.312
Dy_{Si}	229.79	99.48	260.81	8.07	9.22	2186.87	0.433	0.311
Ho_{Si}	231.31	100.70	263.83	8.23	9.36	2200.86	0.435	0.310
Er_{Si}	230.39	102.38	267.51	8.61	9.69	2213.37	0.444	0.306
Tm_{Si}	230.47	104.77	272.94	9.09	10.11	2242.35	0.455	0.303
Yb_{Si}	226.99	106.74	276.82	9.71	10.65	2239.04	0.470	0.297
Lu_{Si}	229.08	111.53	287.87	10.58	11.43	2297.47	0.487	0.291

O_N, respectively. Whereas the variation tendency for the bulk modulus B of β-Si_3N_4 containing NM_N as a function of the atomic number of NM shows the opposite trend to G and E. For RE replacing, the bulk modulus B of β-Si_3N_4 containing RE_{Si} undergo slightly changes, not exceeding 15 GPa, as the atomic number of RE increased, with the average value of 226.28 GPa. Whereas the shear modulus G of β-Si_3N_4 containing RE_{Si} exhibits more pronounced fluctuations with the atomic number, ranging from 233.06 GPa to 297.00 GPa. It initially exhibits a decreasing trend from 297.00 GPa for Sc_{Si} to 233.06 GPa for Ce_{Si}, except for La_{Si} of 294.68 GPa, followed by an increase to 276.51 GPa for Nb_{Si}, and remains relatively stable until reaching Gd_{Si}, after which it drops to 259.90 GPa for Tb_{Si} before gradually increasing again to 287.87 GPa for Lu_{Si}. The Young's modulus E of β-Si_3N_4 containing RE_{Si} demonstrates a similar variation behavior to that of B.

The calculated parameters G/B and ν of β-Si_3N_4 containing

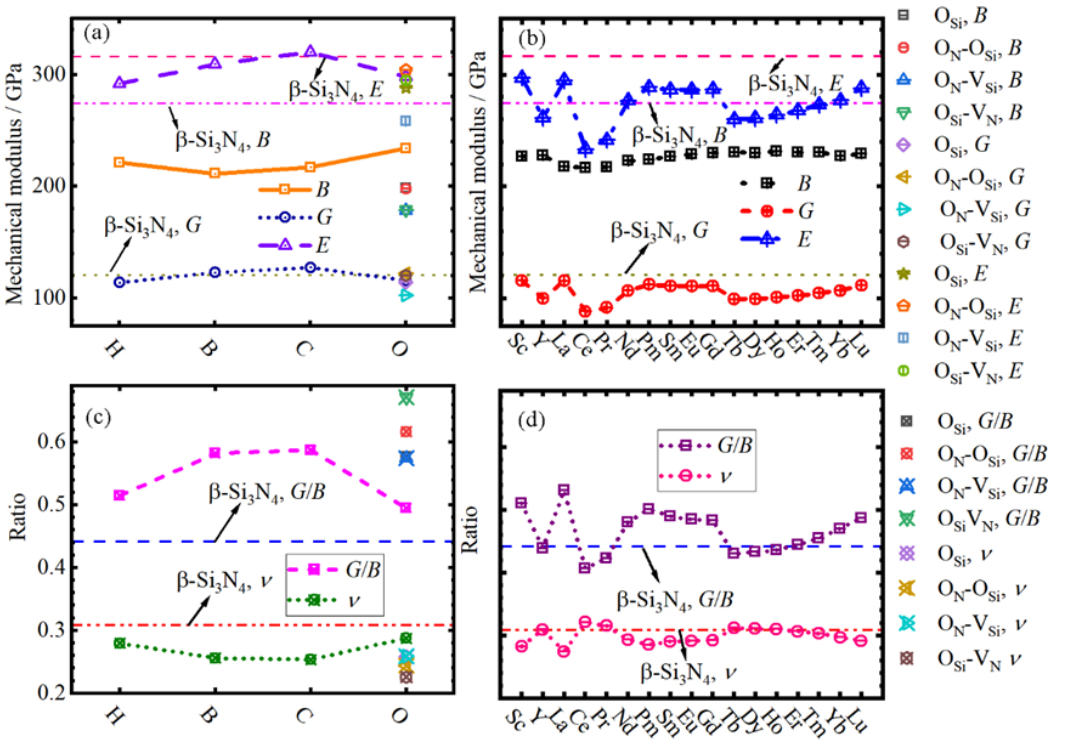

Fig. 2: The bulk modulus B (GPa), shear modulus G (GPa), Young's modulus E (GPa) of (a) NM_N and (b) RE_{Si} as a function of atomic number; The Pugh's modulus ratio G/B and Poisson's ratio ν of (c) NM_N and (d) RE_{Si} as a function of atomic number.

defects NM_N and RE_{Si} as a function of atomic number are illustrated in Fig. 2(c-d). Usually, the Pugh's modulus ratio G/B typically plays a crucial role in determining the brittleness and ductility of polycrystalline materials; that is the higher the value of G/B, the more brittle the materials would be.[61] The ν of greater/smaller than 0.26 is indicative of uniform/nonuniform behaviors response to applied stress. It is seen that the G/B of β-Si_3N_4 containing NM_N firstly increases from 0.51 for H_N to 0.59 for C_N, and then steeply decreases to 0.49 for O_N. Whereas the variation of ν presents the opposite trend. The variation trend of the Pugh's modulus ratio G/B as a function of atomic number of RE is the same as that of moduli E and G of β-Si_3N_4 containing RE_{Si}, while the Poisson's ratio ν exhibits an inverse correlation. Interesting, the G/B of perfect β-Si_3N_4 of 0.441 is larger than that of Y_{Si}, $(Ce\text{-}Pr)_{Si}$, and $(Tb\text{-}Ho)_{Si}$ modified β-Si_3N_4, but lower than the rest RE_{Si}-β-Si_3N_4, indicating that the Y_{Si}, $(Ce\text{-}Pr)_{Si}$, $(Tb\text{-}Ho)_{Si}$ would improve the ductility of β-Si_3N_4.

3.3 The lattice thermal conductivity

Generally, the total TC of a material can be divided into two parts: (1) One part contributed by electrons κ_e. (2) The other part contributed by phonon transport κ_l. However, the TC of pure β-Si_3N_4 only be achieved by the transport as β-Si_3N_4 is a covalent compound whose electrons are bonded and cannot move freely.[65] Thus, the total TC is calculated by $\kappa \approx \kappa_l$. So, the intrinsic TC of β-Si_3N_4 can be affected by the phonon mean free path.[9,11,17,66] A simplified approach involves integrating the spectral specific heat instead of employing the complex phonon Boltzmann equation, as following[38,67-69] Eq. (19):

$$\kappa = \int C(\omega)\, v_s l(\omega) d(\omega) \tag{19}$$

where C, v_s, l, ω are the spectral specific heat, the transverse wave speed, the intrinsic mean free path and frequency of phonon, respectively. And the parameter l, ω are Eq. (20):

$$C(\omega) = \frac{9\kappa_B \omega^2}{N a^3 \omega_m^3}; l(\omega, T) = \left(\frac{G a^3 \nu \omega_m}{2\gamma^2 \omega^2 \kappa_B T}\right) \tag{20}$$

where κ_B, T, γ, N, a^3, ω_m are the Boltzmann constant, Kelvin temperature, Grüneisen parameter the number of atoms per structure, the volume per atom and Debye frequency of acoustic branch, respectively. Thus, from above Eq. (19-20), the κ_l can be rewritten as Eq. (21):

$$\kappa = \left(\frac{3\gamma^2}{2}\right)\left(\frac{G\nu^2}{N\omega_m}\right) T^{-1} \tag{21}$$

Here, the v_s and γ can be obtained from the G and ν, as following[60,70,71] Eq. (22)-(23):

$$v_s = \sqrt{\frac{G}{\rho}};\ \gamma = \frac{3}{2}\left(\frac{1+\nu}{2-3\nu}\right) \tag{22}$$

$$\omega_m = \frac{\theta_D \kappa_B}{h} \tag{23}$$

where h and θ_D is Planck constant and Debye temperature, respectively.

Table 4: The calculated Grüneisen parameter γ, transverse wave speed vs (m/s), Debye temperature θ_D (K) and thermal conductivity κ (W/(m·K)).

Defects	γ	v_s	θ_D	κ
SiN	1.82	6083.15	934.12	272.84; 280 [10] 325.06 [39]; 320 [16]
V_N	1.66	5995.13	915.68	217.11
V_{Si}	1.81	5435.64	832.04	190.15
N_{Si}	1.68	5912.12	906.32	211.87
Si_N	1.60	5997.34	912.75	200.79
H_N	1.66	5931.68	906.79	207.52
B_N	1.53	6160.43	938.03	199.46
C_N	1.52	6260.91	954.16	207.31
O_N	1.70	5954.37	911.50	223.11
O_{Si}	1.54	5955.37	905.75	181.87
O_N-O_{Si}	1.47	6122.35	933.31	181.93
O_N-V_{Si}	1.54	5628.00	856.99	154.73
O_{Si}-V_N	1.39	6088.27	924.38	159.88
Sc_{Si}	1.67	5957.30	909.32	215.15
Y_{Si}	1.83	61595.51	839.22	205.32
La_{Si}	1.62	5847.48	890.09	200.28
Ce_{Si}	1.91	5108.28	781.99	184.19
Pr_{Si}	1.87	5208.83	796.90	187.24
Nd_{Si}	1.73	5615.59	856.90	201.82
Pm_{Si}	1.68	5752.66	877.11	205.73
Sm_{Si}	1.71	5712.60	871.56	208.87
Eu_{Si}	1.72	5702.73	870.36	209.36
Gd_{Si}	1.72	5699.24	870.02	210.93
Tb_{Si}	1.85	5383.19	823.93	204.22
Dy_{Si}	1.84	5390.25	824.97	203.94
Ho_{Si}	1.84	5419.77	829.46	206.10
Er_{Si}	1.81	5461.21	835.50	205.28
Tm_{Si}	1.79	5521.99	844.46	208.05
Yb_{Si}	1.75	5568.29	850.96	205.09
Lu_{Si}	1.72	5689.08	868.80	210.21

The Debye temperature θ_D plays an important role in thermodynamics. A higher θ_D usually directly reflect the better ability of heat conduction.[72,73] It can be calculated as following[73] Eq. (24):

$$\Theta_D = f_\nu \frac{h}{2\pi\kappa_B}(48\pi^5)^{\frac{1}{6}}\sqrt{\frac{r_0 B}{M}} \quad (24)$$

where the M is the atomic weight, the r_0 is the equilibrium Wigner–Seitz radius.

$$f_\nu = \left\{\frac{1}{3}\left[\left[\frac{1+\nu}{3(1-\nu)}\right]^{\frac{3}{2}}\right] + 2\left[\left[\frac{2(1+\nu)}{3(1-2\nu)}\right]^{\frac{3}{2}}\right]\right\}^{-\frac{1}{3}} \quad (25)$$

We have firstly calculated Grüneisen parameter γ, transverse wave speed v_s, Debye temperature θ_D and TC κ of β-Si_3N_4 containing impurities, and the results at room temperature are listed in Table 4. One can see that the calculated value of 272.84 $Wm^{-1}K^{-1}$ for perfect β-Si_3N_4 is lower than other theoretical predictions and experimental values[10,16,39] of ~325.06 $Wm^{-1}K^{-1}$.The reason may be that Eq. (22)-(25) ignore the influence the longitudinal sound velocity and doesn't consider the anharmonic effect. The data from Table 4 reveals that all defects lead to a reduction in the κ of β-Si_3N_4. Notably, among these defects, the presence of O_N-V_{Si} in β-Si_3N_4 results in the lowest κ value recorded at 154.73 W/(m·K). For intrinsic defects, the order of impact of defects on the κ of β-Si_3N_4 is $V_N < N_{Si} < Si_N < V_{Si}$. Clearly, the intrinsic defects V_N, N_{Si}, Si_N, and substitutional defects (H, C, $O)_N$, and (Sc, Y, La, Nd-Lu)$_{Si}$ have the minimal impact on reducing the κ of β-Si_3N_4 and can maintain it up to 200 W/(m·K).

To demonstrate the temperature-dependent TC κ of all defect-β-Si_3N_4 compounds, we present in Fig. 3(a) a graphical representation of κ as a function of temperature (~1000 K). The results show that the κ firstly decreases rapidly when the temperature smaller than 300 K, and then it decreases slowly with increasing temperature to 1000 K. The detailed κ of β-Si_3N_4 containing NM_N and RE_{Si} as a function of atomic number at both 300 and 600 K is given in Fig. 3(b). We can find that the κ of β-Si_3N_4 containing NM_N slowly increases from C_N to O_N. For β-Si_3N_4 containing RE_{Si} defects, the κ initially decreases from Sc_{Si} to Ce_{Si}, then increases to Nd_{Si} and finally stabilizes around 210.93 W/(m·K).

To probe the underlying mechanism, we have investigated the phonon dispersion properties for β-Si_3N_4 containing O_{Si} and Sc_{Si} defects in Fig. 4(b-d) along the path Γ-M-K-Γ-A-L-H-A of high symmetric points with Γ (0, 0, 0), M (0.5, 0, 0), K (0.3, 0.3, 0), A (0, 0, 0.5), L (0.5, 0, 0.5), H (0.3, 0.3 0.5),[74] as illustrated in Fig. 4(a). The results of phonon dispersion for β-Si_3N_4 show a good agreement with values of Zhou *et al*.[75] To analyze the potential effect of defects on TC, we plotted corresponding to the density of states (DOS) curves in the rights of Fig. 4(c-d). In the range of 35 THz), O_{Si} has a more concentrated energy range, while the fluctuations of DOS for Sc_{Si} are more decentralize and smooth, meaning that the stronger anharmonic vibrations lead to a lower TC exhibited in Sc_{Si}.

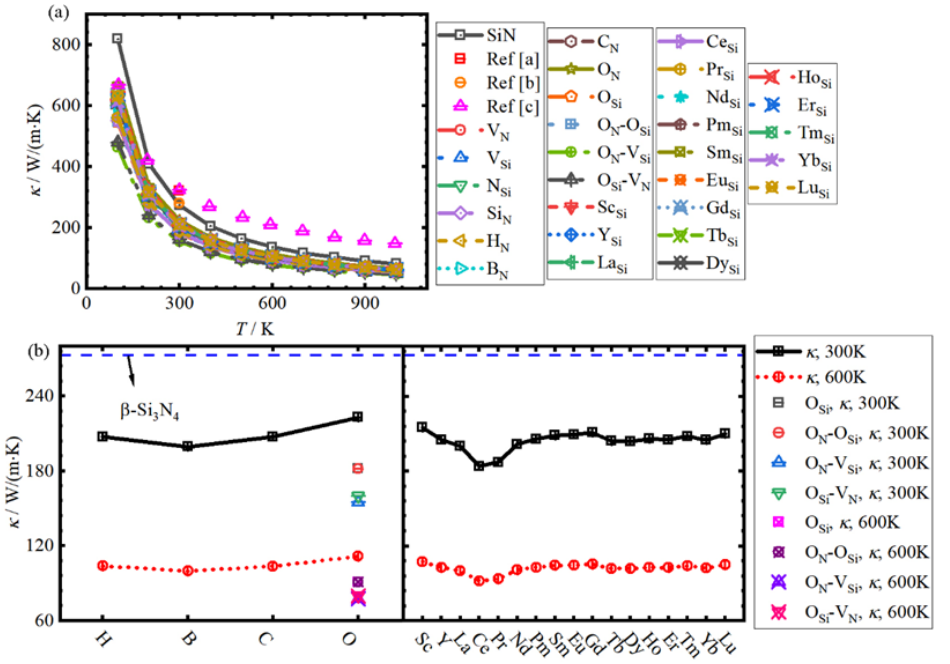

Fig. 3: The calculated thermal conductivity κ as functions of (a) temperature (~1000 K) and (b)atomic atoms, respectively. The reference values of [a] ref.,[16] [b] ref.[10] and ref.[39] are respectively from the experiment, molecular dynamics and first-principles calculations combining with the phonon Boltzmann euqation (BTE).

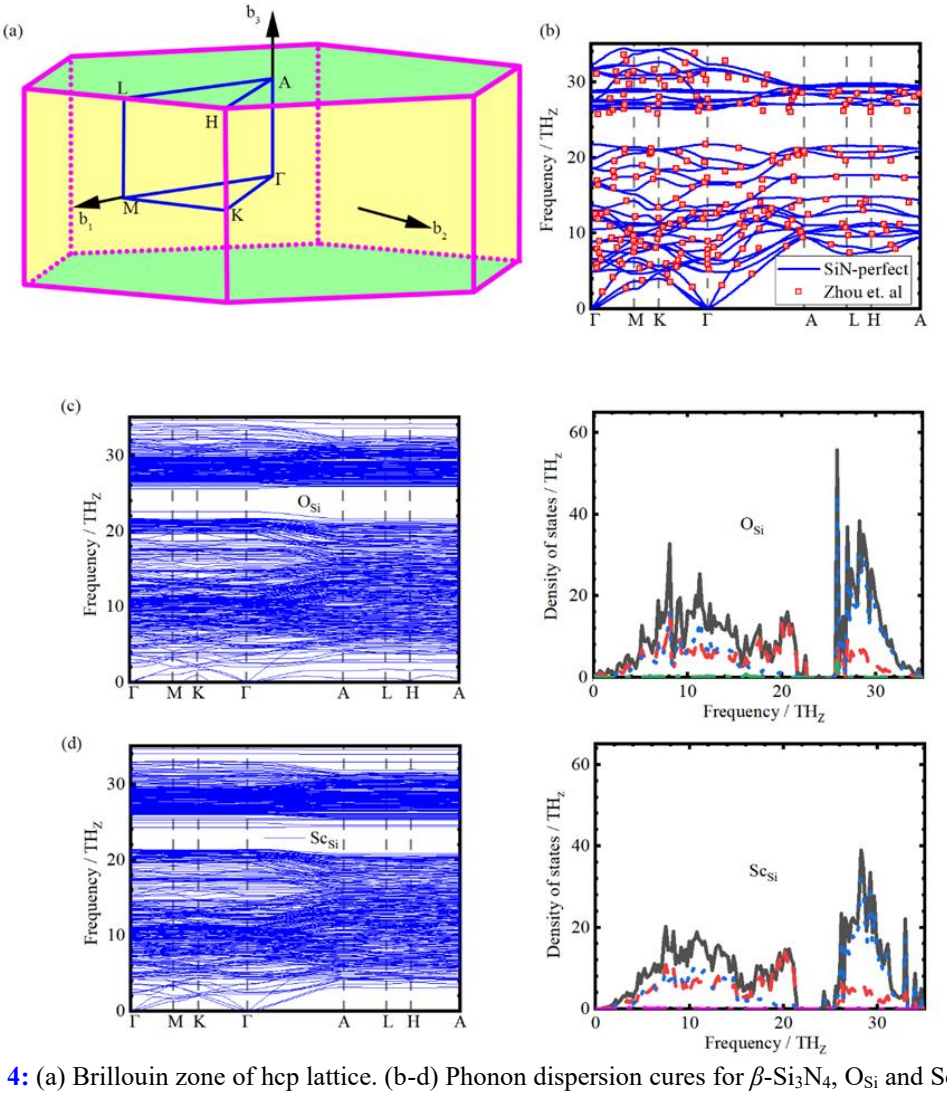

Fig. 4: (a) Brillouin zone of hcp lattice. (b-d) Phonon dispersion cures for β-Si_3N_4, O_{Si} and Sc_{Si}.

3.4 Thermodynamic properties

At present, the first-principles calculations only simulate the properties of materials under the 0 K condition. But properties at finite temperature, such as thermodynamic properties, can be calculated through the first-principles calculations in combination with thermodynamic models. A simple and popular method is often used to obtain thermodynamic parameters by the θ_D. And the entropy S, heat capacity C_V Gibbs free energy G and thermal expansion coefficient α are calculated as:[68,76-78]

$$S = -3n\kappa_B \ln\left(1 - e^{-\frac{\Theta_D}{T}}\right) + 4n\kappa_B D\left(\frac{\Theta_D}{T}\right) \quad (26)$$

$$C_V = 3\kappa_B\left[4D\left(\frac{\Theta_D}{T}\right) - \frac{3\left(\frac{\Theta_D}{T}\right)}{e^{\frac{\Theta_D}{T}} - 1}\right. \quad (27)$$

$$E_g = E_{sta} + \frac{9}{8}n\kappa_B\Theta_D + 3n3n\kappa_B T\ln\left(1 - e^{-\frac{\Theta_D}{T}}\right) - n\kappa_B TD\left(\frac{\Theta_D}{T}\right) \quad (28)$$

$$\alpha = \frac{1}{V}\cdot\frac{dV}{dT} \quad (29)$$

where $Esta$, V and D parameters are the static energy from first-principles calculations, volume and Debye function, $D(y) = \frac{3}{y^3}\int_0^y \frac{x^3}{e^x - 1}dx$ respectively.

The S, C_V, E_g and α of all cases have been calculated using Eq. (26)-(29), and the results are drawn in Fig. 5(a-d) as a function of temperature (0~1000 K). It is seen that the entropy S increases sharply with the temperature increasing to 300K, and then the increasing velocity slows down. Similarly, the C_V,

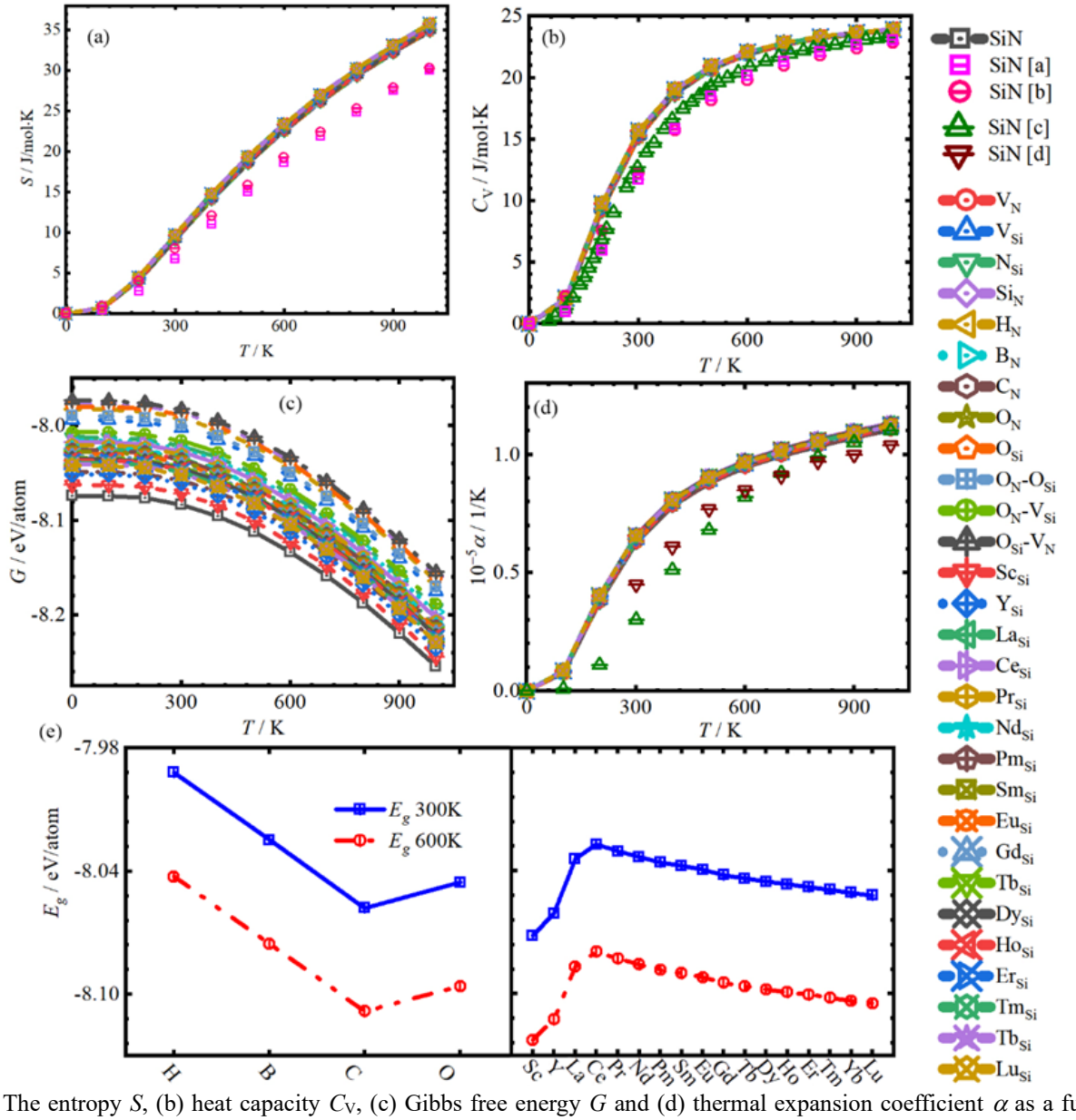

Fig. 5: (a) The entropy S, (b) heat capacity C_V, (c) Gibbs free energy G and (d) thermal expansion coefficient α as a function of temperature; (e) The S, C_V, G and α as a function of atomic number. The values of [a] ref.,[79] [c] ref.[64] and [b] ref.,[80] [d] ref.[81] are respectively the experiment and first-principles.

increases rapidly from 0 to 300 K, and then increases slowly to 1000 K with approaching approximately the Dulong–Petit limit of 25 J/(mol·K). The reason is that the larger value of entropy implies more vibration modes are inspired by the heat, and would provide larger C_V,. Furthermore, the E_g and α respectively show the opposite and same trend compared to S and C_V ,. Clearly, defects would not cause significant difference in S, C_V,, and α, except for E_g. The E_g of perfect β-Si_3N_4 is larger than that of β-Si_3N_4 containing defects in the whole temperature range.

Thus, we plot the E_g of β-Si_3N_4 containing NM_N and RE_{Si} as a function of atomic number in Fig. 5(e). It can be found that the E_g of β-Si_3N_4 containing NM_N decreases from H_N to C_N, and then increases to O_N at both 300 and 600 K. Whereas the E_g of β-Si_3N_4, which contains RE_{Si}, exhibits an increasing trend from Sc_{Si} to Ce_{Si}, and subsequently decreases linearly until Lu_{Si}.

4. Conclusion

Herein, the effects of impurities on the mechanical property and thermal conductivity of β-Si_3N_4 based on the first-principles calculations have been investigated. Clearly, all calculated stability, mechanical, and thermodynamic parameters of NM_N and RE_{Si} exhibit a regular variation with the increasing atomic number. Based on the comprehensive computational results, the incorporation of Sc, Y, and Pm-Lu oxides as sintering aids is expected to preserve the high thermal conductivity of Si_3N_4 while ensuring excellent mechanical properties. The main finding points are as following:

(1) For intrinsic defects, the order of defective formation energy E_f is $V_N < N_{Si} < V_{Si} < Si_N$ in the N-rich side, while in the N-poor side the formation of antisite Si_N becomes facile than the two types before it.

(2) The presence of defects inevitably leads to a reduction in the mechanical modulus (B, G, E) to a certain degree. Interestingly, the Pugh's ratio G/B of pristine β-Si_3N_4 is higher than that of Y_{Si}-, $(Ce\text{-}Pr)_{Si}$-, and $(Tb\text{-}Ho)_{Si}$ defects containing samples, suggesting that the incorporation of Y_{Si}, $(Ce\text{-}Pr)_{Si}$, and $(Tb\text{-}Ho)_{Si}$ enhances the ductility of β-Si_3N_4. Moreover, the group defect O_N-V_{Si} significantly diminishes both the modulus G and E values of β-Si_3N_4.

(3) All defects would lead to a decrease in the thermal conductivity κ of β-Si_3N_4, and among them, intrinsic defects V_N, N_{Si}, Si_N and substitutional defects of $(H, C, O)_N$, $(Sc, Y, La, Nd\text{-}Lu)_{Si}$ have the minimal impact on reducing the κ of β-Si_3N_4 and can maintain it up to 200 W/(m·K).

(4) The defects would not cause significant difference in S, C_V, and α, except for E_g. The E_g of perfect β-Si_3N_4 possesses the largest values in the whole temperature range.

Acknowledgments

This work is supported by the National Natural Science Foundation of China (No. 52371009, 52171115, 52361005), the Xinjiang Development Program for Vanadium-Titanium Magnetite Concentration and Extraction Process Technology (No. 2022LQ01006), the Research Project on Titanium Ore Smelting Process in Xinjiang (No. hmkjxm202206), The Hunan Provincial Natural Science Foundation (2023JJ50320, 2023JJ50109), Hengyang City Guidance Project (2022202015981), and Hunan Provincial Education Department Research Project (23C0400).

Conflict of Interest

The authors declare that they have no known competing financial interests or personal relationships that could have appeared to influence the work reported in this paper.

Supporting Information

Not applicable.

CRediT Statement

Touwen Fan: Conceptualization, Methodology, Formal analysis, Writing-Original draft. **Zixiong Ruan:** Data curation, Software, Investigation, Writing-Original draft. **Yue Hong:** Visualization, Investigation. **Bin Deng:** Resources, Investigation. **Lan Lin:** Software, Validation. **Xianlan Liu:** Visualization, Writing-Review & editing. **Tiansheng Li:** Conceptualization, Funding acquisition, Resources, Supervision, Writing - Review & editing. **Yuanzhi Wu:** Funding acquisition, Resources, Supervision, Writing - Review & editing. **Heng Luo:** Conceptualization, Funding Acquisition, Resources, Supervision, Writing - Review & editing. **Yuanyuan Zhang:** Data curation, Validation.

References

[1] Y. Zhou, H. Hyuga, D. Kusano, C. Matsunaga, K. Hirao, Effects of yttria and magnesia on densification and thermal conductivity of sintered reaction-bonded silicon nitrides, *Journal of the American Ceramic Society*, 2019, **102**, 1579-1588, doi: 10.1111/jace.16015.

[2] Y.-J. Park, M.-J. Park, J.-M. Kim, J.-W. Lee, J.-W. Ko, H.-D. Kim, Sintered reaction-bonded silicon nitrides with high thermal conductivity: The effect of the starting Si powder and Si_3N_4 diluents, *Journal of the European Ceramic Society*, 2014, **34**, 1105-1113, doi: 10.1016/j.jeurceramsoc.2013.11.040.

[3] H. M. Lee, E. B. Lee, D. L. Kim, D. K. Kim, Comparative study of oxide and non-oxide additives in high thermal conductive and high strength Si_3N_4 ceramics, *Ceramics International*, 2016, **42**, 17466-17471, doi: 10.1016/j.ceramint.2016.08.051.

[4] H. Lu, C. Bailey, C. Yin, Design for reliability of power electronics modules, *Microelectronics Reliability*, 2009, **49**, 1250-1255, doi: 10.1016/j.microrel.2009.07.055.

[5] M. Yamagiwa, Packaging technologies of power modules for hybrid electric vehicles and electric vehicles, *Bulletin of the*

Ceramic Society of Japan, 2010, **45**, 432-37, doi: 10.1109/TCPMT.2025.3613928.

[6] C. Buttay, D. Planson, B. Allard, D. Bergogne, P. Bevilacqua, C. Joubert, M. Lazar, C. Martin, H. Morel, D. Tournier, C. Raynaud, State of the art of high temperature power electronics, *Materials Science and Engineering: B*, 2011, **176**, 283-288, doi: 10.1016/j.mseb.2010.10.003.

[7] N. Murayama, K. Hirao, M. Sando, T. Tsuchiya, H. Yamaguchi, High-temperature electro-ceramics and their application to SiC power modules, *Ceramics International*, 2018, **44**, 3523-3530, doi: 10.1016/j.ceramint.2017.11.140.

[8] W. Werdecker, F. Aldinger, Aluminum nitride-an alternative ceramic substrate for high power applications in microcircuits, *IEEE Transactions on Components, Hybrids, and Manufacturing Technology*, 1984, **7**, 399-404, doi: 10.1109/TCHMT.1984.1136380.

[9] Y. Duan, N. Liu, J. Zhang, H. Zhang, X. Li, Cost effective preparation of Si_3N_4 ceramics with improved thermal conductivity and mechanical properties, *Journal of the European Ceramic Society*, 2020, **40**, 298-304, doi: 10.1016/j.jeurceramsoc.2019.10.003.

[10] N. Hirosaki, S. Ogata, C. Kocer, H. Kitagawa, Y. Nakamura, Molecular dynamics calculation of the ideal thermal conductivity of single-crystal α- and β–Si_3N_4, *Physical Review B*, 2002, **65**, 134110, doi: 10.1103/physrevb.65.134110.

[11] K. Hirao, Y. Zhou, H. Hyuga, T. Ohji, D. Kusano, High thermal conductivity silicon nitride ceramics, *Journal of the Korean Ceramic Society*, 2012, **49**, 380-384, doi: 10.4191/kcers.2012.49.4.380.

[12] D. Bose, M. W. Harrington, A. Isichenko, K. Liu, J. Wang, N. Chauhan, Z. L. Newman, D. J. Blumenthal, Anneal-free ultra-low loss silicon nitride integrated photonics, *Light: Science & Applications*, 2024, **13**, 156, doi: 10.1038/s41377-024-01503-4.

[13] B. Palacios–Márquez, Z. Montiel-González, S. A. Pérez-García, M. Moreno, A. Morales–Sánchez, Negative differential resistance and resistive switching behavior in broad-spectrum electroluminescent devices based on Si_3N_4/Si thin films deposited by E-beam, *Applied Surface Science*, 2025, **682**, 161768, doi: 10.1016/j.apsusc.2024.161768.

[14] X. Zhang, Y. Zhou, Y. Zhang, K. Chen, G. Liu, G. Qiao, Theoretical screening and experimental fabrication of metallized layer for enhanced Cu wetting and adhesion on Si_3N_4 substrate, *Ceramics International*, 2025, **51**, 12940-12950, doi: 10.1016/j.ceramint.2025.01.137.

[15] S. Saini, A. Kuriakose, S. Ghosh, P. Srivastava, Highly enhanced and stable field emission performance of CNT–Dielectric (Si_3N_4) hybrids, *Applied Surface Science*, 2024, **652**, 159313, doi: 10.1016/j.apsusc.2024.159313.

[16] J. S. Haggerty, A. Lightfoot, Opportunities for enhancing the thermal conductivities of SiC and Si_3N_4 ceramics through improved processing,, *Ceramic Engineering and Science Proceedings,* 2008, **16**(4), 475-487, doi: 10.1002/9780470314715.ch52.

[17] M. Kitayama, K. Hirao, A. Tsuge, K. Watari, M. Toriyama, S. Kanzaki, Thermal conductivity of β-Si_3N_4: II, effect of lattice oxygen, *Journal of the American Ceramic Society*, 2000, **83**, 1985-1992, doi: 10.1111/j.1151-2916.2000.tb01501.x.

[18] M. Kitayama, K. Hirao, A. Tsuge, M. Toriyama, S. Kanzaki, Oxygen content in ß-Si_3N_4 crystal lattice, *Journal of the American Ceramic Society*, 1999, **82**, 3263-3265, doi: 10.1111/j.1151-2916.1999.tb02238.x.

[19] M. Kitayama, K. Hirao, M. Toriyama, S. Kanzaki, Thermal conductivity of ß-Si_3N_4: I, effects of various microstructural factors, *Journal of the American Ceramic Society*, 1999, **82**, 3105-3112, doi: 10.1111/j.1151-2916.1999.tb02209.x.

[20] C. Jiang, B. P. Uberuaga, S. G. Srinivasan, Point defect thermodynamics and diffusion in Fe3C: a first-principles study, *Acta Materialia*, 2008, **56**, 3236-3244, doi: 10.1016/j.actamat.2008.03.012.

[21] J.-M. Lu, Q.-M. Hu, R. Yang, First-principles investigations of point defect behavior and elastic properties of TiNi based alloys, *MRS Online Proceedings Library*, 2009, **1128**, 903, doi: 10.1557/PROC-1128-U09-03.

[22] J. Li, L. Porter, S. Yip, Atomistic modeling of finite-temperature properties of crystalline β-SiC II. Thermal conductivity and effects of point defects, *Journal of Nuclear Materials*, 1998, **255**, 139-152, doi: 10.1016/S0022-3115(98)00034-8.

[23] Q. Dai, D. He, F. Meng, P. Liu, X. Liu, Dielectric constant, dielectric loss and thermal conductivity of Si_3N_4 ceramics by hot pressing with CeO_2–MgO as sintering aid, *Materials Science in Semiconductor Processing*, 2021, **121**, 105409, doi: 10.1016/j.mssp.2020.105409.

[24] Y. Li, H.-N. Kim, H. Wu, M.-J. Kim, J.-W. Ko, Y.-J. Park, Z. Huang, H.-D. Kim, Enhanced thermal conductivity in Si_3N_4 ceramic with the addition of $Y_2Si_4N_6C$, *Journal of the American Ceramic Society*, 2018, **101**, 4128-4136, doi: 10.1111/jace.15544.

[25] M. Kitayama, K. Hirao, K. Watari, M. Toriyama, S. Kanzaki, Thermal conductivity of β-Si_3N_4: III, effect of rare-earth (RE = La, Nd, Gd, Y, Yb, and Sc) oxide additives, *Journal of the American Ceramic Society*, 2001, **84**(2), 353-58, doi: 10.1111/j.1151-2916.2001.tb00662.x.

[26] H. Yokota, H. Abe, M. Ibukiyama, Effect of lattice defects on the thermal conductivity of β-Si_3N_4, *Journal of the European Ceramic Society*, 2003, **23**, 1751-1759, doi: 10.1016/S0955-2219(02)00374-6.

[27] D. Kusano, H. Hyuga, Y. Zhou, K. Hirao, Effect of aluminum content on mechanical properties and thermal conductivities of

sintered reaction-bonded silicon nitride, *International Journal of Applied Ceramic Technology*, 2014, **11**, 534-542, doi: 10.1111/ijac.12035.

[28] C. Lv, J. Yang, X. Zhang, Y. Cai, X. Liu, G. Wang, S.-N. Luo, Interfacial effect on deformation and failure of Al/Cu nanolaminates under shear loading, *Journal of Physics D: Applied Physics*, 2018, **51**, 335301, doi: 10.1088/1361-6463/aad2a8.

[29] S. Zhao, G. M. Stocks, Y. Zhang, Stacking fault energies of face-centered cubic concentrated solid solution alloys, *Acta Materialia*, 2017, **134**, 334-345, doi: 10.1016/j.actamat.2017.05.001.

[30] P. Chowdhury, H. Sehitoglu, Deformation physics of shape memory alloys–Fundamentals at atomistic frontier, *Progress in Materials Science*, 2017, **88**, 49-88, doi: 10.1016/j.pmatsci.2017.03.003.

[31] H. Van Swygenhoven, P. M. Derlet, A. G. Frøseth, Stacking fault energies and slip in nanocrystalline metals, *Nature Materials*, 2004, **3**, 399-403, doi: 10.1038/nmat1136.

[32] T. W. Fan, Z. P. Wang, J. J. Lin, D. C. Chen, Q. H. Fang, T. Hu, B. H. Nie, K. Wang, H. W. Hu, H. B. Sun, H. Y. He, L. Ma, P. Y. Tang, First-principles predictions for stabilizations of multilayer nanotwins in Al alloys at finite temperatures, *Journal of Alloys and Compounds*, 2019, **783**, 765-771, doi: 10.1016/j.jallcom.2018.12.314.

[33] W. Zhou, X. Ren, Y. Ren, S. Yuan, N. Ren, X. Yang, S. Adu-Gyamfi, Initial dislocation density effect on strain hardening in FCC aluminium alloy under laser shock peening, *Philosophical Magazine*, 2017, **97**, 917-929, doi: 10.1080/14786435.2017.1285073.

[34] J. Hui, X. Zhang, T. Liu, W. Liu, B. Wang, First-principles calculation of twin boundary energy and strength/embrittlement in hexagonal close-packed titanium, *Materials & Design*, 2022, **213**, 110331, doi: 10.1016/j.matdes.2021.110331.

[35] H. Yan, W. Guo, T. Luan, X. Ma, G. Xu, X. Leng, W. Zhao, J. Yan, Strengthening mechanism of Al/Sn interfaces: study from experiments and first-principles calculation, *Materials & Design*, 2021, **212**, 110292, doi: 10.1016/j.matdes.2021.110292.

[36] X. Zhang, Y. Huang, Y. Liu, X. Ren, A comprehensive DFT study on the thermodynamic and mechanical properties of L12-Al_3Ti/Al interface, *Vacuum*, 2021, **183**, 109858, doi: 10.1016/j.vacuum.2020.109858.

[37] X. Lu, J. Luo, P. Yang, J. Ren, X. Guo, P. La, Effects of vacancy on the electronic and optical properties of β-Si_3N_4 by first-principles, *Modern Physics Letters B*, 2019, **33**, 1950451, doi: 10.1142/s0217984919504517.

[38] P. Yang, F. Xu, J. Li, H. Wu, G. Nie, Y. Shao, S. Wu, The impact of oxygen impurity and La doping on thermodynamic properties of Si_3N_4 ceramic: a first-principle calculation approach, *Journal of the European Ceramic Society*, 2020, **40**, 5293-5297, doi: 10.1016/j.jeurceramsoc.2020.07.034.

[39] Y. Li, X. Duan, Z. Fu, H. Zhao, Y.-L. He, X.-L. Lu, J.-Y. Yang, X.-H. Ma, Intrinsic electron mobility and lattice thermal conductivity of β-Si_3N_4 from first-principles, *Solid State Communications*, 2023, **361**, 115066, doi: 10.1016/j.ssc.2023.115066.

[40] S.-S. Li, L. Li, J. Han, C.-T. Wang, Y.-Q. Xiao, X.-D. Jian, P. Qian, Y.-J. Su, First-Principles study on the nucleation of precipitates in ternary Al alloys doped with Sc, Li, Zr, and Ti elements, *Applied Surface Science*, 2020, **526**, 146455, doi: 10.1016/j.apsusc.2020.146455.

[41] Z. Mao, W. Chen, D. N. Seidman, C. Wolverton, First-principles study of the nucleation and stability of ordered precipitates in ternary Al–Sc–Li alloys, *Acta Materialia*, 2011, **59**, 3012-3023, doi: 10.1016/j.actamat.2011.01.041.

[42] J. P. Perdew, K. Burke, M. Ernzerhof, Generalized gradient approximation made simple, *Physical Review Letters*, 1996, **77**, 3865-3868, doi: 10.1103/physrevlett.77.3865.

[43] H. J. Monkhorst, J. D. Pack, Special points for Brillouin-zone integrations, *Physical Review B*, 1976, **13**, 5188-5192, doi: 10.1103/physrevb.13.5188.

[44] R. P. Feynman, Forces in molecules, *Physical Review*, 1939, **56**, 340-343, doi: 10.1103/physrev.56.340.

[45] K. Momma, F. Izumi, *VESTA*: a three-dimensional visualization system for electronic and structural analysis, *Journal of Applied Crystallography*, 2008, **41**, 653-658, doi: 10.1107/s0021889808012016.

[46] A. Kuwabara, K. Matsunaga, I. Tanaka, Lattice dynamics and thermodynamical properties of silicon nitride polymorphs, *Physical Review B*, 2008, **78**, 064104, doi: 10.1103/physrevb.78.064104.

[47] X. Zhu, S. Zhang, T. Li, H. Tang, L. Wang, Y. Yu, Z. Qiao, Computational and experimental analysis of the optical properties of β-Si_3N_4 doped Be, Ca, Ba and Eu, *Solid State Communications*, 2022, **358**, 115000, doi: 10.1016/j.ssc.2022.115000.

[48] P. Ravindran, L. Fast, P. A. Korzhavyi, B. Johansson, J. Wills, O. Eriksson, Density functional theory for calculation of elastic properties of orthorhombic crystals: Application to TiSi$_2$, *Journal of Applied Physics*, 1998, **84**, 4891-4904, doi: 10.1063/1.368733.

[49] V. Wang, N. Xu, J.-C. Liu, G. Tang, W.-T. Geng, VASPKIT: a user-friendly interface facilitating high-throughput computing and analysis using VASP code, *Computer Physics Communications*, 2021, **267**, 108033, doi: 10.1016/j.cpc.2021.108033.

[50] Y. Le Page, P. Saxe, Symmetry-general least-squares extraction of elastic coefficients from *ab initio* total energy calculations, *Physical Review B*, 2001, **63**, 174103, doi:

10.1103/physrevb.63.174103.
[51] Z.-J. Wu, E.-J. Zhao, H.-P. Xiang, X.-F. Hao, X.-J. Liu, J. Meng, Crystal structures and elastic properties of superhard IrN_2 and IrN_3 from first principles, *Physical Review B*, 2007, **76**, 054115, doi: 10.1103/physrevb.76.054115.
[52] R. Hill, The elastic behaviour of a crystalline aggregate, *Proceedings of the Physical Society A*, 1952, **65**, 349-354, doi: 10.1088/0370-1298/65/5/307.
[53] Z. Chen, P. Zhang, D. Chen, Y. Wu, M. Wang, N. Ma, H. Wang, First-principles investigation of thermodynamic, elastic and electronic properties of Al_3V and Al_3Nb intermetallics under pressures, *Journal of Applied Physics*, 2015, **117**, 085904, doi: 10.1063/1.4913664.
[54] A. Hao, X. Yang, X. Wang, Y. Zhu, X. Liu, R. Liu, First-principles investigations on electronic, elastic and optical properties of XC (X=Si, Ge, and Sn) under high pressure, *Journal of Applied Physics*, 2010, **108**, 063531, doi: 10.1063/1.3478717.
[55] X.-Q. Chen, H. Niu, D. Li, Y. Li, Modeling hardness of polycrystalline materials and bulk metallic glasses, *Intermetallics*, 2011, **19**, 1275-1281, doi: 10.1016/j.intermet.2011.03.026.
[56] C. Li, Z. Wang, First-principles study of structural, electronic, and mechanical properties of the nanolaminate compound Ti_4GeC_3 under pressure, *Journal of Applied Physics*, 2010, **107**, 123511, doi: 10.1063/1.3446096.
[57] Y. Deng, O.-H. Jia, X.-R. Chen, J. Zhu, Phase transition and elastic constants of CaO from first-principle calculations, *Physica B: Condensed Matter*, 2007, **392**, 229-232, doi: 10.1016/j.physb.2006.11.023.
[58] J. Wei, L. Zhang, Y. Liu, First-principles calculations study the mechanical and thermal properties of Cr–Al–B ternary borides, *Solid State Communications*, 2021, **326**, 114182, doi: 10.1016/j.ssc.2020.114182.
[59] C. Chen, S. Fan, J. Niu, H. Huang, Z. Jin, L. Kong, D. Zhu, G. Yuan, Alloying design strategy for biodegradable zinc alloys based on first-principles study of solid solution strengthening, *Materials & Design*, 2021, **204**, 109676, doi: 10.1016/j.matdes.2021.109676.
[60] T. Jia, G. Chen, Y. Zhang, Lattice thermal conductivity evaluated using elastic properties, *Physical Review B*, 2017, **95**, 155206, doi: 10.1103/PhysRevB.95.155206.
[61] R. Vogelgesang, M. Grimsditch, J. S. Wallace, The elastic constants of single crystal β-Si_3N_4, *Applied Physics Letters*, 2000, **76**, 982-984, doi: 10.1063/1.125913.
[62] G. A. Swift, E. Üstündag, B. Clausen, M. A. M. Bourke, H.-T. Lin, High-temperature elastic properties of *in situ*-reinforced Si_3N_4, *Applied Physics Letters*, 2003, **82**, 1039-1041, doi: 10.1063/1.1554478.
[63] B. H. Yu, D. Chen, Y. L. Jia, Pseudo-potential calculations of structural, elastic and thermal properties of Si_3N_4, *Advanced Materials Research*, 2011, **217-218**, 1619-1624, doi: 10.4028/www.scientific.net/amr.217-218.1619.
[64] S. F. Pugh, XCII. Relations between the elastic moduli and the plastic properties of polycrystalline pure metals, *The London, Edinburgh, and Dublin Philosophical Magazine and Journal of Science*, 1954, **45**, 823-843, doi: 10.1080/14786440808520496.
[65] F. Hu, Z.-P. Xie, J. Zhang, Z.-L. Hu, D. An, Promising high-thermal-conductivity substrate material for high-power electronic device: silicon nitride ceramics, *Rare Metals*, 2020, **39**, 463-478, doi: 10.1007/s12598-020-01376-7.
[66] M. Kitayama, K. Hirao, A. Tsuge, M. Toriyama, S. Kanzaki, Oxygen content in ß-Si_3N_4 crystal lattice, *Journal of the American Ceramic Society*, 1999, **82**, 3263-3265, doi: 10.1111/j.1151-2916.1999.tb02238.x.
[67] P. G. Klemens, Phonon scattering by oxygen vacancies in ceramics, *Physica B: Condensed Matter*, 1999, **263**, 102-104, doi: 10.1016/S0921-4526(98)01202-2.
[68] A. Togo, I. Tanaka, First principles phonon calculations in materials science, *Scripta Materialia*, 2015, **108**, 1-5, doi: 10.1016/j.scriptamat.2015.07.021.
[69] H. Xiang, J. Wang, Y. Zhou, Theoretical predictions on intrinsic lattice thermal conductivity of ZrB_2, *Journal of the European Ceramic Society*, 2019, **39**, 2982-2988, doi: 10.1016/j.jeurceramsoc.2019.04.011.
[70] D. S. Sanditov, V. N. Belomestnykh, Relation between the parameters of the elasticity theory and averaged bulk modulus of solids, *Technical Physics*, 2011, **56**, 1619-1623, doi: 10.1134/S106378421111020X.
[71] V. N. Belomestnykh, E. P. Tesleva, Interrelation between anharmonicity and lateral strain in quasi-isotropic polycrystalline solids, *Technical Physics*, 2004, **49**, 1098-1100, doi: 10.1134/1.1787679.
[72] C. Toher, J. J. Plata, O. Levy, M. de Jong, M. Asta, M. B. Nardelli, S. Curtarolo, High-throughput computational screening of thermal conductivity, Debye temperature, and Grüneisen parameter using a quasiharmonic Debye model, *Physical Review B*, 2014, **90**, 174107, doi: 10.1103/physrevb.90.174107.
[73] Y. Zhang, First-principles Debye–Callaway approach to lattice thermal conductivity, *Journal of Materiomics*, 2016, **2**, 237-247, doi: 10.1016/j.jmat.2016.06.004.
[74] W. Setyawan, S. Curtarolo, High-throughput electronic band structure calculations: Challenges and tools, *Computational Materials Science*, 2010, **49**, 299-312, doi: 10.1016/j.commatsci.2010.05.010.
[75] H. Zhou, T. Feng, Theoretical upper limits of the thermal conductivity of Si_3N_4, *Applied Physics Letters*, 2023, **122**, 182203, doi: 10.1063/5.0149298.
[76] Z. Zhou, B. Wu, S. Dou, C. Zhao, Y. Xiong, Y. Wu, S. Yang, Z. Wei, Thermodynamic properties of elements and compounds

in Al-Sc binary system from *ab initio* calculations based on density functional theory, *Metallurgical and Materials Transactions A*, 2014, **45**, 1720-1735, doi: 10.1007/s11661-013-2117-9.
[77] D. N. Talwar, J. C. Sherbondy, Thermal expansion coefficient of 3C–SiC, *Applied Physics Letters*, 1995, **67**, 3301-3303, doi: 10.1063/1.115227.
[78] L. J. Porter, J. Li, S. Yip, Atomistic modeling of finite-temperature properties of β-SiC. I. Lattice vibrations, heat capacity, and thermal expansion, *Journal of Nuclear Materials*, 1997, **246**, 53-59, doi: 10.1016/S0022-3115(97)00035-4.
[79] B.-H. Yu, D. Chen, Predictions of pressure-induced structural transition, mechanical and thermodynamic properties of α- and β-Si_3N_4ceramics: *ab initio* and quasi-harmonic Debye modeling, *Chinese Physics B*, 2012, **21**, 060508, doi: 10.1088/1674-1056/21/6/060508.
[80] J. A. Wendel, W. A. Goddard III, The Hessian biased force field for silicon nitride ceramics: Predictions of thermodynamic and mechanical properties for α- and β-Si_3N_4, *The Journal of Chemical Physics*, 1992, **97**, 5048-5062, doi: 10.1063/1.463859.
[81] I.C. Huseby, G.A. Slack, R.H. Arendt, Thermal Expansion of $CdAl_2O_4$ *β*-Si_3N_4, and other phenacite-type compounds, *American Ceramic Society Bulletin*, 1981, **60**, 919-954, doi: 10.1063/1.330070.